

# NJC

Accepted Manuscript



This is an *Accepted Manuscript*, which has been through the Royal Society of Chemistry peer review process and has been accepted for publication.

*Accepted Manuscripts* are published online shortly after acceptance, before technical editing, formatting and proof reading. Using this free service, authors can make their results available to the community, in citable form, before we publish the edited article. We will replace this *Accepted Manuscript* with the edited and formatted *Advance Article* as soon as it is available.

You can find more information about *Accepted Manuscripts* in the [Information for Authors](#).

Please note that technical editing may introduce minor changes to the text and/or graphics, which may alter content. The journal's standard [Terms & Conditions](#) and the [Ethical guidelines](#) still apply. In no event shall the Royal Society of Chemistry be held responsible for any errors or omissions in this *Accepted Manuscript* or any consequences arising from the use of any information it contains.



NJC

PERSPECTIVE

## Recent progress in hybrid cathode materials for lithium ion batteries

Chuanliang Wei, Wen He,\* Xudong Zhang,\* Jianxing Shen and Jingyun Ma

Received 00th January 20xx,  
Accepted 00th January 20xx

DOI: 10.1039/x0xx00000x

www.rsc.org/

Rechargeable lithium ion batteries (LIBs) are considered as one of the most promising power sources for electric vehicles (EVs) and hybrid electric vehicles (HEVs) applications due to their high energy density, durable cycle life, higher output power and safety issues. Previous research mainly focuses on a single electrode. However, a single cathode material is difficult to meet requirements for EVs and HEVs. So the concept of “hybrid cathode material” was proposed. The so-called hybrid cathode material combines a number of excellent electrochemical properties of each cathode material and has become an alternative to the conventional single cathode material. The present study of hybrid cathode materials is mainly focused on the composite of two kinds of cathode materials. In this review, we summarize the recent progress in hybrid cathode materials, such as  $\text{LiFePO}_4\text{-Li}_3\text{V}_2(\text{PO}_4)_3$ ,  $\text{LiFePO}_4\text{-LiCoO}_2$ ,  $\text{LiFePO}_4\text{-LiMn}_2\text{O}_4$ ,  $\text{LiFePO}_4\text{-LiVPO}_4\text{F}$ ,  $\text{LiFePO}_4\text{-LiMnPO}_4$ ,  $\text{Li}_3\text{V}_2(\text{PO}_4)_3\text{-LiMnPO}_4$ ,  $\text{Li}_3\text{V}_2(\text{PO}_4)_3\text{-LiVPO}_4\text{F}$ ,  $\text{Li}_3\text{V}_2(\text{PO}_4)_3\text{-LiVOPO}_4$  and  $\text{LiCoO}_2\text{-LiMn}_2\text{O}_4$ . A prospective of hybrid cathode materials is also discussed.

### Introduction

As we know, vehicles are playing an increasingly important role in our modern life. However, with the decreasing of oil resource and the declining of environmental quality, looking for new energy sources for vehicles to replace oil has become a problem that the humanity has to face. In recent years, natural gas has been used in some cars. However, exhaust gas emitted by cars still increases the burden of environment, which may limit its further application. Electrical energy as a clean energy has become the first energy choice for vehicles, because it can be converted from three major renewable sources: wind, solar and hydroelectric.<sup>1</sup> In order to store electrical energy used for vehicles, rechargeable batteries are required.

Rechargeable lithium ion batteries (LIBs) are considered as one of the most promising power sources for electric vehicles (EVs) and hybrid electric vehicles (HEVs) applications due to their high energy density, durable cycle life, higher output power and safety issues.<sup>2,3</sup> A LIB mainly consists of a negative electrode (anode) and a positive electrode (cathode) separated and connected by a  $\text{Li}^+$  conducting electrolyte.<sup>4</sup> Cathode materials are one of the most important components of LIBs and play a critical role in determining the performance of LIBs.<sup>5</sup> In the past few years, many cathode materials have been reported, such as  $\text{LiCoO}_2$ ,<sup>6-12</sup>  $\text{LiMn}_2\text{O}_4$ ,<sup>13-15</sup>  $\text{LiMnPO}_4$ ,<sup>16-20</sup>  $\text{LiTi}_2(\text{PO}_4)_3$ ,<sup>21-23</sup>  $\text{LiFePO}_4$ ,<sup>24-33</sup>  $\text{Li}_3\text{V}_2(\text{PO}_4)_3$ ,<sup>34-41</sup>  $\text{LiVPO}_4\text{F}$ <sup>42,43</sup> and  $\text{LiVOPO}_4$ .<sup>44-46</sup>

Shandong Key Laboratory of Glass and Functional Ceramic, Qilu University of Technology, Jinan 250353, China. E-mail: [hewen1960@126.com](mailto:hewen1960@126.com); [zxd10z80@126.com](mailto:zxd10z80@126.com); Fax: +86 53189631518; Tel: +86 531 89631080



Chuanliang Wei graduated from Qilu University of Technology in 2012. In 2013, he moved to the Institute of Materials Science and Engineering, Qilu University of Technology as a postgraduate student, and majored in materials science and engineering.



Wen He is currently a full professor in the Department of Materials Science and Engineering at Qilu University of Technology. She received her PhD degree of Materials Science from South China University of Technology in 2009. Her research interests focus on material chemistry and technology for lithium batteries.

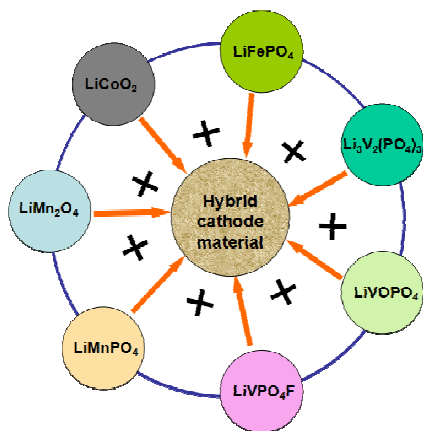


**Fig. 1** Hybrid cathode materials for lithium ion batteries.

The superior cathode materials should meet the following requirements: (1) high theoretical capacity; (2) high operating voltage; (3) high energy density; (4) high tap density; (5) long cycle life; (6) good rate performance; (7) good electrochemical and thermal stability; (8) low cost; (9) safety and environmental friendliness. However, a single cathode material has difficulties to meet the above-mentioned requirements. In order to solve this problem, the concept of “hybrid cathode material” was proposed. The so-called hybrid cathode material (Fig. 1) is a composite that combines the advantages of two or more cathode materials. The hybrid cathode material may be an alternative to the conventional single cathode material. The present study of hybrid cathode materials is mainly focused on the composite of two cathode materials.

Herein, we present a review specially on the recent progress in hybrid cathode materials for LIBs in the past few years. Various hybrid cathode materials such as  $\text{LiFePO}_4\text{-Li}_3\text{V}_2(\text{PO}_4)_3$ ,  $\text{LiFePO}_4\text{-LiCoO}_2$ ,  $\text{LiFePO}_4\text{-LiMn}_2\text{O}_4$ ,  $\text{LiFePO}_4\text{-LiVPO}_4\text{F}$ ,  $\text{LiFePO}_4\text{-LiMnPO}_4$ ,  $\text{Li}_3\text{V}_2(\text{PO}_4)_3\text{-LiMnPO}_4$ ,  $\text{Li}_3\text{V}_2(\text{PO}_4)_3\text{-LiVPO}_4\text{F}$ ,  $\text{Li}_3\text{V}_2(\text{PO}_4)_3\text{-LiVOPO}_4$  and  $\text{LiCoO}_2\text{-LiMn}_2\text{O}_4$  are summarized and analyzed. A prospective of hybrid cathode materials is also discussed.

### $\text{LiFePO}_4\text{-Li}_3\text{V}_2(\text{PO}_4)_3$

Since  $\text{LiFePO}_4$  (LFP) was first reported by Goodenough et al.,<sup>47</sup> LFP was considered as one of the most promising cathode materials for LIBs due to its high theoretical capacity ( $170 \text{ mAh g}^{-1}$ ), cycling stability, low cost and environmental friendliness.<sup>48</sup> Nowadays, among all the lithium transition metal phosphates such as  $\text{LiMPO}_4$  ( $\text{M}=\text{Fe, Co, Ni, Mn}$ ),  $\text{LiVOPO}_4$  and  $\text{Li}_3\text{V}_2(\text{PO}_4)_3$ , only LFP has been successfully commercialized. However, although the theoretical capacity of LFP is  $170 \text{ mAh g}^{-1}$ , the first attempts to de-insert Li from LFP were limited to about  $0.6 e^-$  owing to transport limitations of electrons and ions.<sup>47</sup> Lithium motion in the olivine crystal structure occurs through one-dimensional channels, with little possibility of crossing between channels.<sup>49</sup> LFP usually shows a poor rate capability because of its low intrinsic electronic

conductivity ( $1.8 \times 10^{-9} \text{ S cm}^{-1}$ ) and slow  $\text{Li}^+$  diffusion ( $10^{-16}\text{--}10^{-14} \text{ m}^2 \text{ s}^{-1}$ ).<sup>50,56</sup> The working voltage (about 3.4 V) and tap density of LFP are relatively low, and  $\text{Fe}^{2+}$  in LFP is easily oxidized to  $\text{Fe}^{3+}$  in the process of calcination. All the above-mentioned drawbacks limit the further development and utilization of LFP.

Monoclinic  $\text{Li}_3\text{V}_2(\text{PO}_4)_3$  (LVP) is another potential cathode material for LIBs, because it possesses high theoretical capacity ( $197 \text{ mAh g}^{-1}$ ), high operating voltage (about 4 V) and safety performance.<sup>57–59</sup> The 3D path created by  $\text{PO}_4^{3-}$  units in LVP enables a three dimensional pathway for Li ion insertion/extraction, in contrast to the one dimensional Li ion pathway demonstrated in LFP.<sup>60,61</sup> Compared with LFP, monoclinic LVP possesses superior electrical conductivity ( $2.4 \times 10^{-7} \text{ S cm}^{-1}$ ) and ionic conductivity ( $10^{-9}\text{--}10^{-8} \text{ S cm}^{-1}$ ), which enables Li ions to intercalate and deintercalate effortlessly.<sup>62–64</sup> Although LVP has a higher voltage, it invariably suffers from its stepped voltage platforms and severe cycle attenuation, especially under high voltage.<sup>65–67</sup>

It is obvious that LFP and LVP have their own advantages and drawbacks. In order to integrate the advantages of LFP and LVP, hybrid cathode materials between LFP and LVP have become a research hotspot in recent years. The reasons may be that: (1) a high reversible capacity and high operating voltage of LVP can ensure the high energy density for hybrid cathode materials; (2) a better ion mobility of LVP is expected to facilitate the excellent rate performance of hybrid cathode materials. The co-existence of V-doped LFP and Fe-doped LVP plays great role in electrons transfer activity and lithium ion diffusivity in hybrid cathode materials.<sup>68,69</sup> To date, a series of LFP-LVP hybrid cathode materials have been reported. In order to simplify the synthesis process and improve the

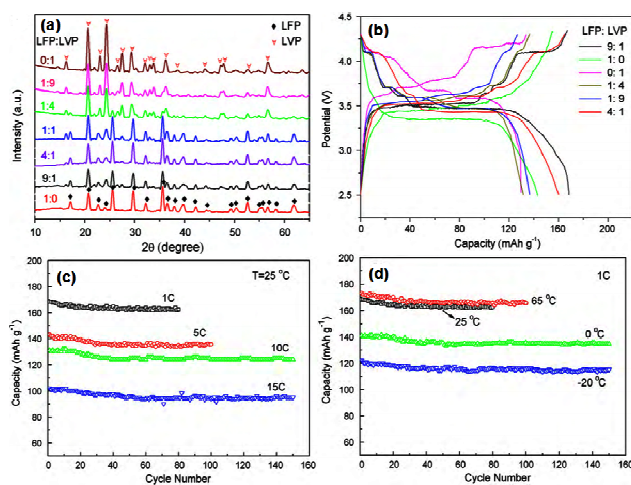


**Fig. 2** (a) XRD patterns of  $x\text{LFP} \cdot y\text{LVP}/\text{C}$  composites. (b) The initial charge-discharge curves of  $x\text{LFP} \cdot y\text{LVP}/\text{C}$  composites. (c) Cycling performances of  $9\text{LFP} \cdot \text{LVP}/\text{C}$  at different discharge rates. (d) Cycling performances of  $9\text{LFP} \cdot \text{LVP}/\text{C}$  at different working temperatures. Reproduced with permission from ref. 70. Copyright 2010 Elsevier.

NJC

electrochemical properties of the electrode material, Xiang et al.<sup>70</sup> reported a simple solid-state synthesis of xLFP·yLVP/C composites using micro-size petroleum coke as both reduction agent and carbon source. The as-prepared material is not a simple mixture of LFP and LVP, but a composite possessing two phases: one is V-doped LFP and the other is Fe-doped LVP. Fig. 2a shows the XRD patterns of as-prepared xLFP·yLVP/C. When x:y=1:0 and 0:1, all the diffraction peaks correspond well to orthorhombic LFP and monoclinic LVP, respectively. When x:y=9:1, 4:1, 1:1, 1:4 and 1:9, both the peaks of orthorhombic LFP and monoclinic LVP appear in the XRD patterns of the as-prepared materials. Besides, no diffraction peaks of carbon are detected in all the products, indicating the state of coated carbon is amorphous or the carbon quantity is too small to be detected. Fig. 2b shows the initial charge-discharge curves of xLFP·yLVP/C composites at 1 C (charge rate:  $1C_{xLFP, yLVP}=(170x+132y)/(x+y)$  mA g<sup>-1</sup>) in 2.5–4.3 V. It can be seen that all the composites show similar charge-discharge behaviors. In the charging process, long plateaus around 3.5 V is corresponding to the phase transition from LiFePO<sub>4</sub> to FePO<sub>4</sub>. The three subsequent plateaus around 3.6, 3.7 and 4.1 V can be indexed to the transformation of Li<sub>3</sub>V<sub>2</sub>(PO<sub>4</sub>)<sub>3</sub> to Li<sub>2.5</sub>V<sub>2</sub>(PO<sub>4</sub>)<sub>3</sub>, Li<sub>2.5</sub>V<sub>2</sub>(PO<sub>4</sub>)<sub>3</sub> to Li<sub>2</sub>V<sub>2</sub>(PO<sub>4</sub>)<sub>3</sub> and Li<sub>2</sub>V<sub>2</sub>(PO<sub>4</sub>)<sub>3</sub> to LiV<sub>2</sub>(PO<sub>4</sub>)<sub>3</sub>, respectively.<sup>58</sup> Obviously, different contents of LFP and LVP phases in the composites have various electrochemical performances. Among all the composites, the 9LFP·LVP/C composite exhibits the highest discharge capacity of 168 mAh g<sup>-1</sup> and initial coulombic efficiency of 98%. The cycling performances of 9LFP·LVP/C at different rates and working temperatures are shown in Fig. 2c and d. At rates of 1, 5, 10 and 15 C, the initial discharge capacity of 9LFP·LVP/C is 168, 143, 131 and 102 mAh g<sup>-1</sup>, respectively. The discharge capacity is 163 mAh g<sup>-1</sup> at 1 C after 80 cycles and 125 mAh g<sup>-1</sup> at 10 C after 150 cycles, respectively. Moreover, at the temperature of 65, 0 and -20 °C, the reversible capacity of 9LFP·LVP/C is 166, 134 and 115 mAh g<sup>-1</sup>, respectively. Even after 150 cycles at -20 °C, the capacity of 9LFP·LVP/C still sustains 75% of that at room temperature. The improved electrochemical performances of 9LFP·LVP/C are greatly attributed to the enhanced electrical conductivity. The electrical conductivity of 9LFP·LVP/C is improved to  $2.50 \times 10^{-2}$  S cm<sup>-1</sup>, much higher than those of pristine LFP/C ( $6.75 \times 10^{-3}$  S cm<sup>-1</sup>) and LVP/C

( $2.88 \times 10^{-3}$  S cm<sup>-1</sup>). It is also suggested that the excellent cycling performances at high rate and wide working temperature range are attributed to the interaction of V-doped LFP and Fe-doped LVP in the composite, which increase the electronic conductivity and facilitate the insertion/extraction of lithium ions.

The V resources or Fe resources used to synthesize LFP-LVP composite are often different. The most commonly used V resources are V<sub>2</sub>O<sub>5</sub> and NH<sub>4</sub>VO<sub>3</sub>, and the most commonly used Fe resources are Fe<sub>2</sub>O<sub>3</sub> and FeCl<sub>3</sub>. Different starting materials usually lead to different synthesis methods, so the method to synthesize LFP-LVP composite is various. Recently, Zheng et al.<sup>71</sup> reported a new way to synthesize LFP-LVP composite cathode material. Firstly, they used NH<sub>4</sub>VO<sub>3</sub> and Fe(NO<sub>3</sub>)<sub>3</sub> as the starting materials to synthesize fine precursor FeVO<sub>4</sub>, then synthesized LFP-LVP composite by chemical reduction and lithiation. Fig. 3a shows the XRD pattern of LFP-LVP composite synthesized at 700 °C for 12 h. It can be seen that the diffraction peaks of the synthesized composite are composed of both LFP and LVP, indicating the synthesized composite is a mixture of LFP and LVP. Fig. 3b shows the initial charge-discharge curves of LFP-LVP/Li cells at different rates in the potential range of 2.5–4.5 V. The curves all contain four plateaus, with three plateaus for LVP and the other one for LFP. As seen in Fig. 3c, the initial discharge capacity of LFP-LVP composite is about 142.5, 138.4 and 123.4 mAh g<sup>-1</sup> at the rate of 0.1, 1 and 3 C, respectively, and the corresponding discharge capacity is about 139.1, 135.5 and 116 mAh g<sup>-1</sup> after 30 cycles.

Polyol process is considered as an encouraging process to synthesize LFP with wonderful electrochemical performances. The polyol medium itself acts not only as a solvent in the process but also as a stabilizer, limiting particle growth and prohibiting agglomeration. Moreover, the polyol process provides a reducing environment, which is extremely advantageous for synthesizing LFP, because it is difficult to obtain divalent iron containing LFP.<sup>69,72</sup> To get LFP·LVP composite with excellent electrochemical performances, Gao et al.<sup>69</sup> successfully synthesized LFP·LVP/C composite via a polyol process. They used citric acid and polyethylene glycol (PEG) as carbon sources, and triethylene glycol (TEG) as both a

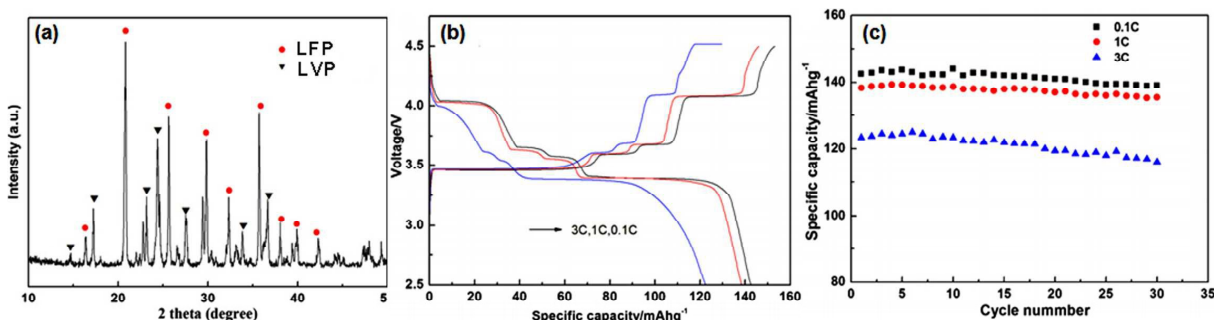


**Fig. 3** (a) XRD pattern of LFP-LVP composite. (b) Initial charge-discharge curves of LFP-LVP at different rates in 2.5–4.5 V. (c) Cycling performances of LFP-LVP composite. Reproduced with permission from ref. 71. Copyright 2010 Elsevier.

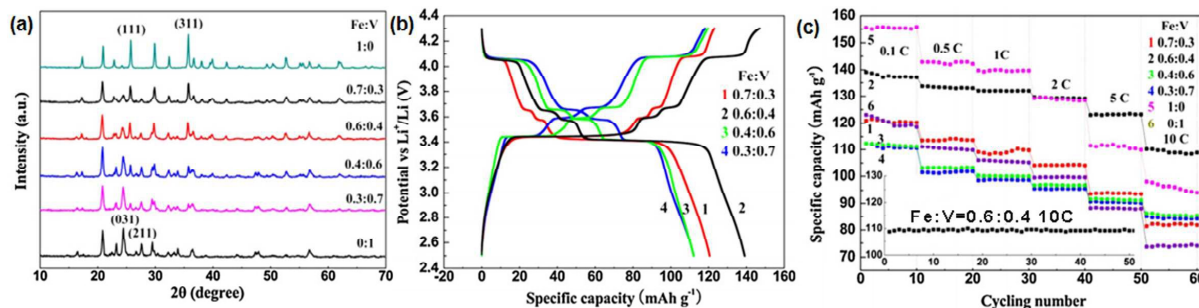


**Fig. 4** (a) XRD patterns of as-prepared materials synthesized at 650 °C for 2 h. (b) Charge-discharge curves of as-prepared materials at 0.1 C in 2.5–4.3 V. (c) Cycling performances of as-prepared materials at different rates in voltage range of 2.5–4.3 V. Reproduced with permission from ref. 69. Copyright 2013 Elsevier.

**Table 1** LFP-LVP hybrid cathode materials for LIBs.

Molar ratio	Preparation method	Electrochemical performances	References
Fe:V=1:1	Solution method	In 2.5–4.3 V, 100 mAh g <sup>-1</sup> at 10 C.	73
LFP:LVP=8:1	Rheological phase reaction method	In 2.0–4.4 V, 151 mAh g <sup>-1</sup> (second cycle) at 1 C.	74
LFP:LVP=5:1	Chemical reduction and lithiation method	In 2.5–4.5 V, initial discharge capacity of 165 mAh g <sup>-1</sup> at 0.1 C.	68
LFP:LVP=5:1	Polyethylene glycol (PEG)-assisted rheological phase method	In 2.5–4.5 V, initial discharge capacities of 134.8 and 129.9 mAh g <sup>-1</sup> at 1 and 2 C, respectively.	75
LFP:LVP=7:3	Sol-gel method	In 2.5–4.5 V, initial discharge capacity of 166 mAh g <sup>-1</sup> at 0.1 C, remaining 127 mAh g <sup>-1</sup> at 10 C and 109 mAh g <sup>-1</sup> at 20 C.	76
LFP:LVP=9:1	Spray-drying and post-calcining method	In 2.5–4.5 V, initial discharge capacities of 161.3, 153.3, 147.6, 135.3 and 109.6 mAh g <sup>-1</sup> at 0.1, 1, 2, 5 and 10 C, respectively.	77
LFP:LVP=9:1	Sol-gel method	In 2.5–4.5 V, initial discharge capacity of 131.3 mAh g <sup>-1</sup> and capacity retention of 95.1% after 200 cycles at 10 C.	78
LFP:LVP=9:1	Sol-gel method	In 2.5–4.5 V, initial discharge capacities of 162.19, 160.92, 154.40, 149.02, 134.85 and 104.99 mAh g <sup>-1</sup> at 0.1, 0.5, 1, 2, 5 and 10 C, respectively.	79
LFP:LVP=9:1	Sol-gel combustion method	In 2.4–4.2 V, initial discharge capacities of 153.1, 137.7, 113.6 and 93.3 mAh g <sup>-1</sup> at 1, 2, 5 and 10 C, respectively.	80
LFP:LVP=3:1	Sol spray drying method	In 2.5–4.5 V, initial discharge capacities of 152.0, 134.3 and 116.8 mAh g <sup>-1</sup> at 1, 5 and 10 C, and capacity retentions of 99.2, 98.2 and 97.7% after 100 cycles, respectively.	81
Fe:V=0.95:0.05	Modified solid-state method	In 2.5–4.2 V, initial discharge capacities of 165.2 and 135.4 mAh g <sup>-1</sup> at 0.1 and 1 C, respectively. With no noticeable capacity fading after 100 cycles at 1 C (141.6 mAh g <sup>-1</sup> ).	48
LFP:LVP=2:1	Spray drying method	In 2.5–4.5 V, initial discharge capacities of 147.6, 145.0, 141.0, 134.1 and 123.0 mAh g <sup>-1</sup> at 0.1, 1, 2, 5 and 10 C, respectively.	82

solvent and a reductant. The XRD patterns of as-prepared pristine LFP/C, pristine LVP/C and xLFP·yLVP/C composites are shown in Fig. 4a. The patterns of pristine LFP/C and pristine LVP/C are in agreement with those of PDF (019-721) and PDF (053-1027), respectively. The diffraction peaks of xLFP·yLVP/C are composed of both LFP and LVP peaks, and no other phase was checked. Fig. 4b shows the initial charge-discharge curves of xLFP·yLVP/C composites at 0.1 C rate in 2.5–4.3 V. Four plateaus are detected in all charge curves. The first plateaus

around 3.4 V is attributed to the Li<sup>+</sup> insertion/extraction of LFP, other three plateaus around 3.60, 3.68 and 4.08 V are connected with Li<sup>+</sup> insertion/extraction of LVP. It can be seen from Fig. 4b that the discharge capacity of LF<sub>0.6</sub>P·LV<sub>0.4</sub>P/C composite is 140 mAh g<sup>-1</sup>, while those of other xLFP·yLVP/C composite are less than 130 mAh g<sup>-1</sup>. Fig. 4c shows the cycling performances of pristine LFP/C, pristine LVP/C and xLFP·yLVP/C composites at different rates (0.1, 0.5, 1, 2, 5 and 10 C). The pristine LFP/C exhibits the highest discharge capacities of

NJC

155, 145, 140 and 130 mAh g<sup>-1</sup> at 0.1, 0.5, 1 and 2 C, respectively. However, the LF<sub>0.6</sub>P<sub>1</sub>LV<sub>0.4</sub>P/C exhibits the highest discharge capacities of 125 and 110 mAh g<sup>-1</sup> at 5 and 10 C, respectively. Furthermore, the discharge capacity remains 110 mAh g<sup>-1</sup> after 50 cycles at 10 C and the coulombic efficiency is almost 100% at 10 C in the 50 cycles. They predicted the combination of Fe<sup>2+</sup>-doped LVP/C and V<sup>3+</sup>-doped LFP/C was supposed as the main factor to the high rate performance of LF<sub>0.6</sub>P<sub>1</sub>LV<sub>0.4</sub>P/C composite.

More details about LFP-LVP hybrid cathode materials for LIBs are summarized in Table 1.

From what we described above, we can get that different proportions of Fe and V have different electrochemical performances, and the same proportions of Fe and V may also have various electrochemical performances, which can be attributed to different synthetic methods. However, few reports paid attention to the theoretical specific capacity of LFP-LVP hybrid cathode materials. In general, LVP is usually allowed to extract and insert two lithium ions reversibly to prevent the decomposition of electrolyte (<4.5 V). In this case, the theoretical specific capacity of the LFP-LVP composite will increase with the increase of LFP. Because in this charge-discharge potential range (usually 2.0–4.5 V), the theoretical capacity of LFP (170 mAh g<sup>-1</sup>) is higher than that of LVP (133 mAh g<sup>-1</sup>). Although the discharge capacity of LFP-LVP hybrid cathode materials may be not as well as single LFP, the overall electrochemical performances of LFP-LVP hybrid cathode materials are superior than single LFP or single LVP in some respects, such as high rate performance, electrical conductivity, ionic conductivity and average working voltage, because the hybrid cathode materials combine the advantages of both LFP and LVP.

Obviously, LFP-LVP hybrid cathode materials have been studied a lot in the past few years. However, problems still exist. The composite mechanism between LFP and LVP is still controversial. The final product is solid solution or just a simple mixture between LFP and LVP. How to get an optimal proportion between LFP and LVP is still a problem, and need much more research work. The future workers should pay

more attention to the modification work of LFP-LVP hybrid cathode materials. Firstly, an optimal proportion between LFP and LVP should be determined. Then, various modification methods such as carbon coating, ion doping, nanocrystallization and controlling morphologies should be adopted to improve the electrochemical performances of LFP-LVP hybrid cathode materials. Furthermore, the synthetic methods also need to be considered.

#### LiFePO<sub>4</sub>-LiCoO<sub>2</sub>

Layered structure LiCoO<sub>2</sub> (LCO) is the first commercialized cathode material in LIBs and has been used in most commercial LIBs. LCO has ease of preparation, high energy density, high operational voltage, good cycleability and good electrochemical performance at elevated temperature with charging voltage lower than 4.2 V.<sup>83,84</sup> LCO could deliver a specific capacity of 140 mAh g<sup>-1</sup> when charged up to 4.2 V versus Li<sup>+</sup>/Li. In fact, LCO has a high theoretical capacity of 274 mAh g<sup>-1</sup>, in order to obtain higher capacity, it needs to be charged above 4.2 V.<sup>85-87</sup> However, its capacity fades quickly when the charging voltage is beyond 4.2 V, which is attributed to structural instability and/or irreversible phase transition.<sup>88-89</sup> Doping or coating is an effective method to improve the performance of LCO.

As we described before, LFP has many advantages and already achieved industrialization. Considering that the coating of LCO by LFP may improve both the thermal stability and electrochemical performance of LCO, Wang et al.<sup>83</sup> prepared LFP-coated LCO by impregnation method. Fig. 5a shows the XRD patterns of the bare and 5.0 wt.% LFP-coated LCO. Obvious diffraction patterns of crystalline LFP can be found in 5.0 wt.% LFP-coated LCO (labeled by # in Fig. 5a), indicating that the coating layer is crystalline LFP. Fig. 5b shows the charge-discharge curves of the bare and LFP-coated cathodes at 1 C in 2.5–4.2 V. The discharge capacity of the bare cathode dropped from 140 to 88 mAh g<sup>-1</sup> after 50 cycles, while

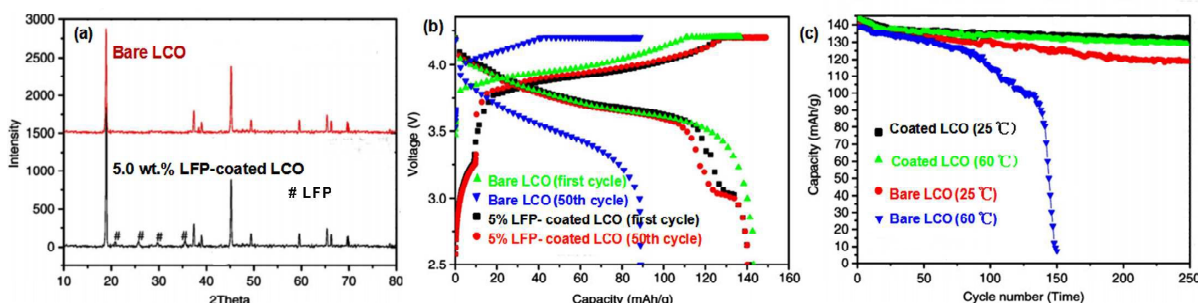


**Fig. 5** (a) XRD patterns of the bare and 5.0 wt.% LFP-coated LCO. (b) Charge-discharge curves of the bare and 5.0 wt.% LFP-coated LCO cathodes at 1 C in 2.5 – 4.2 V at 65 ° C. (c) Cycling performances of the bare and 5.0 wt.% LFP-coated LCO cathodes at charge-cutoff voltages of 4.2 V at 1 C rate at 25 ° C and 60 ° C. Reproduced with permission from ref. 83. Copyright 2007 Elsevier.

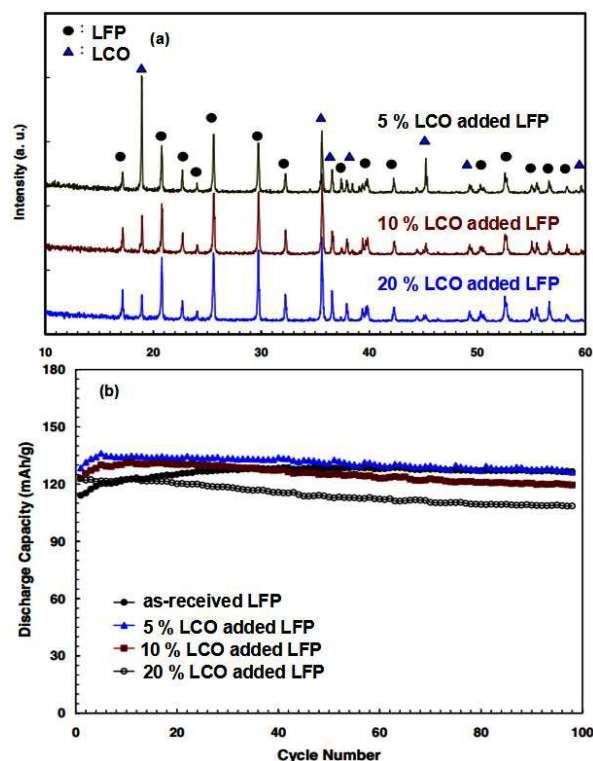


**Fig. 6** (a) X-ray diffraction patterns of LCO-added LFP powder. (b) Cycling performances of as-received LFP and LCO-added LFP at a current rate of 0.5 C in 2.0–4.0 V. Reproduced with permission from ref. 84. Copyright 2009 Springer.

there was almost no capacity loss after 50 cycles for the coated cathode. Unlike other usually used coating materials such as MgO, ZrO<sub>2</sub>, TiO<sub>2</sub> or Al<sub>2</sub>O<sub>3</sub>, the LFP coating layer is not only an active cathode material but also a protecting layer for the LCO, which results in an improved electrochemical performance. In order to examine the chemical stability of the coating layer, the cycling performances of the bare and LFP-coated LCO were tested and the result was shown in Fig. 5c. After 250 cycles at cutoff voltage of 4.2 V at 60 °C, the capacity fading rate of the coated cathode material is only 8.5%, while it is about 95% after only 150 cycles when using the bare LCO as the cathode material. For comparison, the capacity retention of the bare cathode is 85% after 250 cycles when cycled at 25 °C. This indicated that the LFP coating layer was not corroded during cycling at 60 °C and did not lose its protective effect to LCO. The result also indicated that the LFP layer was strong enough to protect the core material from being exposed to the electrolyte at higher operating temperature.

Nanocrystallization, doping cations and coating a conductive layer on the surface of LFP are three commonly used methods for improving the low electric conductivity of LFP. So the low electric conductivity of LFP material may be improved by adding LCO to LFP. In order to improve the poor electrical conductivity of LFP, Kim et al.<sup>84</sup> synthesized a mixed

cathode using a solid state method by adding LCO to LFP. Fig. 6a shows the XRD patterns of the mixed electrodes prepared from the LFP powder with 5, 10, 20 wt.% of LCO added, respectively. When 5 wt.% of LCO was added, the (003) peak was observed around 18°, and when 10 wt.% was added, the (006)/(012), (108)/(110), (101), (104) of the layered peak started to become observable.<sup>90</sup> However, the peak changes in XRD patterns do not indicate the formation of other compounds, but that two compounds were mixed physically with each other. Fig. 6b shows the cycling performances of as-received LFP and LCO-added LFP at a current rate of 0.5 C in 2.0–4.0 V. It can be seen from Fig. 6b that the initial discharge capacity of the bare-LFP material was maintained even after 100 cycles, proving its excellent cycling performance. And the mixed electrode added with 5 wt.% of LCO also shows very good cycling performance, similar to the bare-LFP active material. The mixed electrode with 10 wt.% of LCO added still showed a very good cycling performance, although it did show a small decrease in discharge capacity during charge-discharge cycle. However, the 20 wt.% LCO-added mixed electrode started to show slightly capacity fading after ten charge-discharge cycles. The reason why capacity fading increases on the 20 wt.% LCO-added mixed electrode is that the cycling performance of LCO is lower than that of LFP. They finally concluded that the higher the ratio of LCO, up to 10 wt.%, that is added to the LFP material, the better the rate capability of the mixed electrode, and the more its thermal stability and cycling performance are degraded.

Compared to LFP-LVP hybrid cathode materials, the reports about LFP-LCO are relatively few. The reasons are various. The structures of LFP and LCO are different, which may affect the homogeneity of hybrid cathode materials. LCO and LFP have already achieved industrialization and used in many electronic devices, so adding LFP to LCO (or adding LCO to LFP) to improve the performances of LCO (or LFP) may be not so important. The synthetic process of LFP-LCO cathode materials is also complex. Furthermore, safety issues, high cost, toxicity and environmental concerns limit the further development of LCO.

#### LiFePO<sub>4</sub>-LiMn<sub>2</sub>O<sub>4</sub>

Spinel LiMn<sub>2</sub>O<sub>4</sub> (LMO) cathode material for LIBs has been extensively investigated due to its low cost and low toxicity. Spinel LMO which has three-dimensional lithium diffusion paths is considered as a potentially attractive alternative to the presently commercialized LCO.<sup>91</sup> It has a high discharge voltage plateau of approximately 4.0 V and a theoretical reversible capacity of approximately 148 mAh g<sup>-1</sup>. However, severe capacity and cycling performance fading during cycling prohibit LMO from commercialization.<sup>92,93</sup> In order to improve the electrochemical performances of LMO, Sadeghi et al.<sup>91</sup> coated LMO cathode with nanostructured LFP layer. Firstly, spinel LMO particles was synthesized by solid-state reaction, then the surface of these particles was modified by nanostructured LFP via sol gel dip coating method. The LFP modified LMO can be protected from Mn dissolution, because the LFP nanostructure is formed on the surface of the spinel LMO cathode. Fig. 7a

NJC

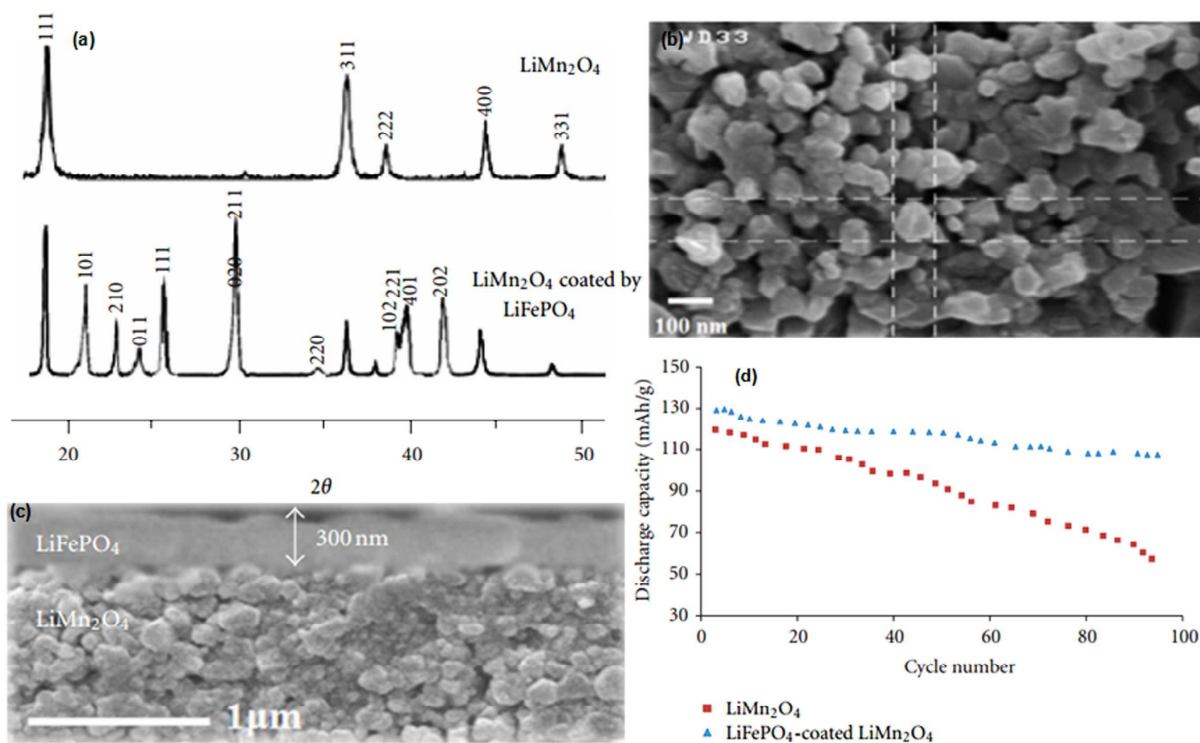


**Fig. 7** (a) XRD patterns of uncoated bare LMO and LMO coated with LFP. (b) Surface SEM image. (c) Cross-section SEM image of LFP thin film deposited on LMO substrate. (d) Cycling performances of bare LMO and LMO coated with LFP at 1 C in 3.0–4.3 V. Reproduced with permission from ref. 91. Copyright 2012 Hindawi.

shows XRD patterns of uncoated bare LMO and LMO coated with LFP. The lattice constants of bare LMO and modified LMO were calculated from the XRD spectrums which are 0.821 and 0.823 nm, respectively. Obviously, the modified samples have a larger lattice constant than bare spinel. LFP may form not only a thin layer on the surface of spinel but also a solid solution by interacting with spinel.<sup>94</sup> In addition, the decrease in the lattice parameter of the modified sample may be due to substitute iron ion with manganese. The increase of lattice constant can make the crystal structure more stable, leading to the stable cycling performance of LFP-modified LMO during charge-discharge process. Fig. 7b and c shows the SEM images of surface and cross-section of LFP thin film deposited on LMO substrate, respectively. As can be seen in Fig. 7c, the thickness of film is about 300 nm. Fig. 7d shows the cycling performances of bare LMO and LMO coated with LFP at 1 C in 3.0–4.3 V. It is obvious that surface modification significantly improves the cyclability of LMO. The presence of LFP phosphate layer not only leads to a better electrical conductivity of LMO particles, but also lower or hinder the additional reactions of cathode materials with the electrolyte. All in all, this improves the cyclic capacity of the battery at the higher rates and also results in higher discharge rates of cathode materials of LMO coated with phosphate layer of LFP.

In consideration of that spinel LMO and olivine LFP are competitive and complementary to each other, and they have their own merits relative to their counterparts when compared with one another, Qiu et al.<sup>95</sup> prepared LMO/LFP blends by hand milling and ball milling using commercial LFP and LMO. Fig. 8a shows the XRD patterns of commercial LMO and LFP samples. It can be seen that the XRD pattern of LMO can be indexed well on the cubic spinel structure (space group  $Fd\bar{3}m$ ) and the XRD pattern of LFP fits well with that of orthorhombic olivine-type structure with space group of  $Pnma$ . In order to study the effects of mass ratio on the electrochemical performances of the blend cathodes, LMO/LFP blends with mass fractions of LMO varied from 100%, 80%, 50%, 20% and 0 were prepared by hand milling. The samples are denoted as LFP-0, LFP-0.2, LFP-0.5, LFP-0.8 and LFP-1.0, respectively. Fig. 8b compares the cycling performances of the LMO/LFP blend electrodes. It is obvious that LMO (LFP-0) has much better cycle stability than LFP (LFP-1.0). The cycling performance of LFP-0.2 or LFP-0.5 electrode is as well as that of LMO electrode. However, the discharge capacity gradually decreases with further addition of LFP (LFP-0.8). Based on the above observations, the LFP-0.5 sample seems to be the best one which provides not only a high discharge capacity but also a good cycle stability.

The capacity fading of LMO seems to be more serious than LFP. Coating LMO with a LFP layer may be an effective method to solve this problem. However, LMO is usually

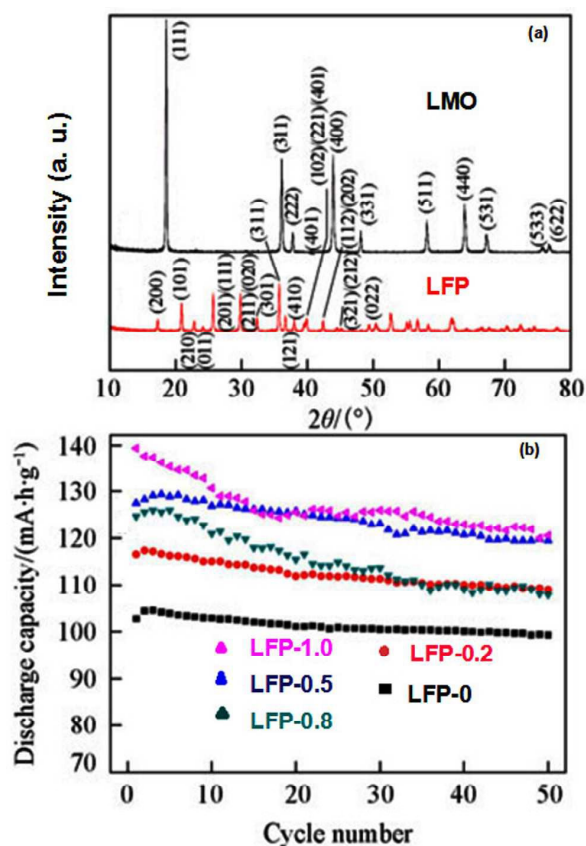


**Fig. 8** (a) XRD patterns of commercial LMO and LFP samples. (b) Cycling performances of LMO/LFP blend electrodes. Reproduced with permission from ref. 95. Copyright 2015 HIGHER EDUCATION PRESS.

calcined in air atmosphere, and LFP is usually calcined in inert gas atmosphere. The different calcination atmosphere between LFP and LMO may be an unfavorable factor for synthesizing LFP-LMO hybrid cathode materials. Enough reducing agent is required in the calcining process of LFP, while too much reducing agent will inhibit the formation of LMO. So LFP and LMO are usually synthesized separately, then are mixed by ball milling. Future workers should pay attention to this problem.

#### LiFePO<sub>4</sub>-LiVPO<sub>4</sub>F

LiVPO<sub>4</sub>F (LVPF) is considered as one of the most promising cathode materials for the development of power LIBs due to its high rate capability, high working potential, excellent cycling performance, stable structure and high thermal stability against electrolyte.<sup>96,97</sup> The theoretical specific capacity of LVPF for lithium deintercalation/reintercalation is about 156 mA h g<sup>-1</sup>.<sup>98</sup> The flat voltage plateau at about 4.2 V (vs. Li/Li<sup>+</sup>) suggests a typical two-phase reaction mechanism during charge/discharge.<sup>99</sup> LVPF compound is isostructural with the naturally occurring mineral tavorite, LiFePO<sub>4</sub>·OH, crystallizing with a triclinic structure.<sup>100,101</sup> Furthermore, the

thermal stability and specific energy of LVPF are superior to LFP.<sup>102,103</sup> However, LVPF exposed to air/moisture is difficult to avoid the surface oxidation and moisture-absorption, which will result in the structural changes of LVPF. As a result, it may show poor electrochemical performance due to partial vanadium oxidation and/or lithium and fluorine loss.<sup>104,105</sup>

As described above, LVPF has a working potential of 4.2 V vs. Li<sup>+</sup>/Li, which is within the electrochemical window of conventional, carbonate-based, non-aqueous electrolytes and is slightly higher than that of LFP (4.1 V vs. Li<sup>+</sup>/Li).<sup>42</sup> In order to raise the operating voltage of LFP, Lin et al.<sup>101</sup> introduced LVPF to prepare xLFP·(1-x)LVPF [x:(1-x)]=1:0, 0.99:0.01, 0.75:0.25, 0.5:0.5, 0.25:0.75 and 0:1] composites through an aqueous precipitation and carbothermal reduction method. Fig. 9a shows the XRD patterns of two-component xLFP·(1-x)LVPF powders with different mole ratios of x:(1-x). When x=1 and 0, the diffraction pattern exhibits a pure phase of LFP and LVPF, respectively. When x:(1-x)=0.99:0.01, there are no second phases or impurities found in the diffraction pattern. The co-existing phases of LFP and LVPF are observed for the LFP-LVPF (x=0.75, 0.5 and 0.25) composites, respectively. Among all the LFP-LVPF composites, the LFP-LVPF (x=0.99) composite demonstrated the best discharge capacity with a flat discharge plateau at about 3.4 V vs. Li/Li<sup>+</sup> and a slight voltage polarization of about 0.06 V between two plateaus at 0.1 C rate, as shown in Fig. 9b. The LFP-LVPF (x=0.99) composite achieved a reversible capacity of 160 mA h g<sup>-1</sup> at 0.2 C. Fig. 9c and d show the charge-discharge curves of pure LFP and LVPF at different rates, respectively. It is clear that the charge-discharge performance of LFP-LVPF (x=0.99) is much better than pure LFP or LVPF.

The reports about LFP-LVPF hybrid cathode materials are limited. The synthesis condition of LVPF is very strict. Moreover, the toxicity of fluorine and vanadium limit its further development.

#### LiFePO<sub>4</sub>-LiMnPO<sub>4</sub>

In addition to the above-mentioned hybrid cathode materials, many other hybrid cathode materials consisting of LFP have also been reported, such as LiFePO<sub>4</sub>-LiMnPO<sub>4</sub> (LFP-LMP).<sup>106,107</sup>

Based on the fact that coating the members of the olivine family LMP with conductive carbon is difficult, excepted in the case M=Fe, Zaghib et al.<sup>106</sup> coated LMP with a thin layer of LFP to take benefit of the catalytic reaction of Fe with C, and a 3 nm-thick layer of carbon can be deposited at the surface of this composite. The carbon coating on top of the LFP layer is shown in Fig. 10. Fig. 10 also illustrates that the interface between LMP and LFP is sharp. The strains at the interface between the two materials are accommodated by extended defects such as the dislocation outlined by the circle in the figure. Moreover, the LFP layer is well crystallized. They found that the electrochemical properties of the carbon-coated LFP-LMP composite were improved

NJC

with respect to the carbon-coated  $\text{LiMn}_{2/3}\text{Fe}_{1/3}\text{PO}_4$  solid solution with comparable Fe/Mn ratio.

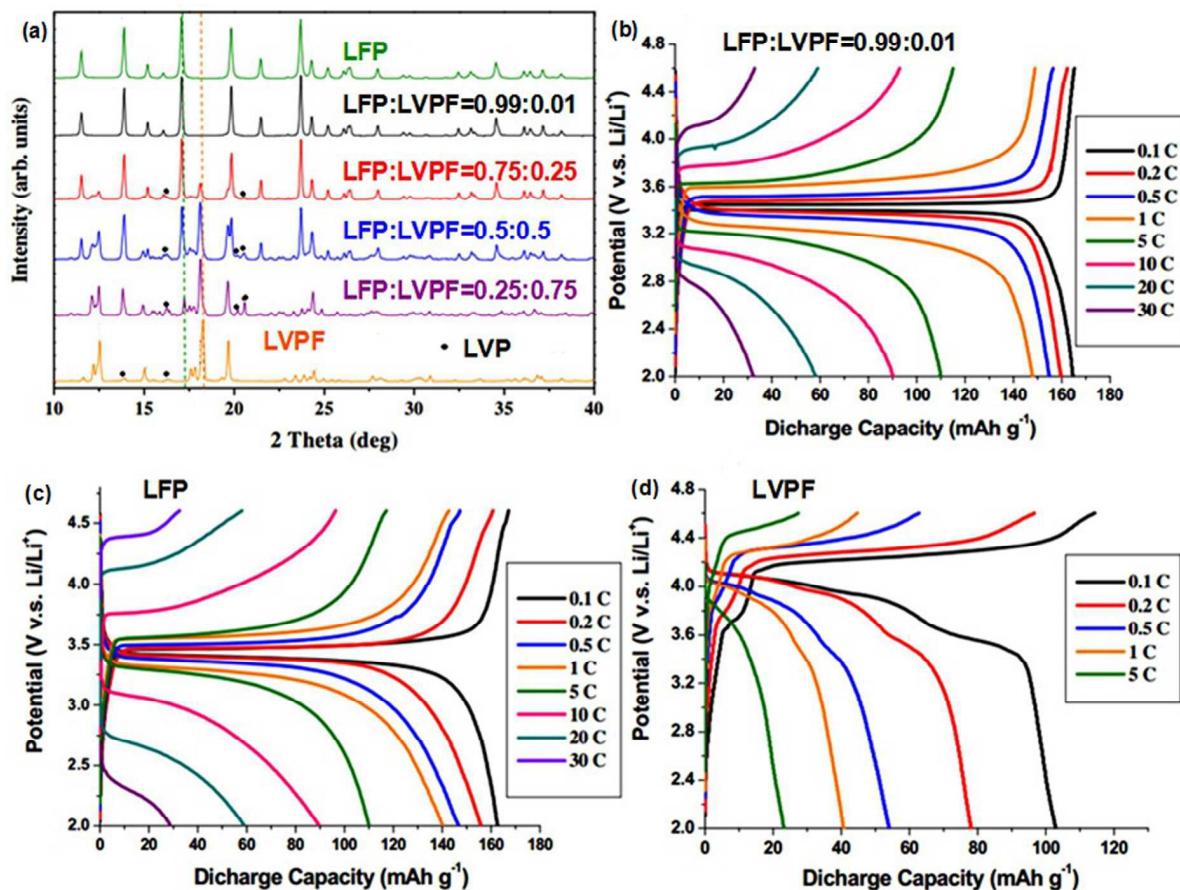


**Fig. 9** (a) XRD patterns of  $x\text{LFP} \cdot (1-x)\text{LVPF}$  composites with different mole ratios of  $x:(1-x)$ . (b) Charge-discharge curves of  $\text{LFP-LVPF}$  ( $x=0.99$ ) composites at different rates. (c) Charge-discharge curves of pure LFP at different rates. (d) Charge-discharge curves of pure LVPF at different rates. Reproduced with permission from ref. 101. Copyright 2013 Elsevier.

### $\text{Li}_3\text{V}_2(\text{PO}_4)_3\text{-LiMnPO}_4$

$\text{LiMnPO}_4$  (LMP) as another promising member among olivine phosphates gains more and more attentions from researchers. Compared with the commercially successful LFP, LMP has the similar theoretical capacity of  $171 \text{ mAh g}^{-1}$ , but can provide about 20% higher energy density than LFP due to its higher redox potential of  $\text{Mn}^{3+}/\text{Mn}^{2+}$  (4.1 V) than  $\text{Fe}^{3+}/\text{Fe}^{2+}$  (3.5 V).<sup>47</sup> Moreover, the 4.1 V intercalation potential of LMP is compatible with conventional nonaqueous organic electrolytes of lithium ion batteries.<sup>108</sup> However, just like LFP, LMP suffers from poor electronic conductivity ( $<10^{-10} \text{ S cm}^{-1}$ ) and low lithium diffusivity due to the heavy polaronic holes localized on the  $\text{Mn}^{3+}$  sites (the Jahn-Teller ion) and the interfacial strain between the  $\text{LiMnPO}_4$  and  $\text{MnPO}_4$  phase.<sup>109-111</sup>

Based on that the low cost LMP with highly conducting LVP may bring up some synergistic effects and result in the

superior electrochemical activity, Wang et al.<sup>112</sup> synthesized a series of  $x\text{LMP} \cdot y\text{LVP/C}$  ( $x/y=1:0, 8:1, 4:1, 2:1, 1:1$  and  $0:1$ ) composites by spray drying followed by solid-state reaction using sucrose as the carbon source and reductive agent. Fig. 11a shows the XRD patterns of the  $x\text{LMP} \cdot y\text{LVP/C}$  ( $x/y=1:0, 8:1, 4:1, 2:1, 1:1$  and  $0:1$ ) composites. It can be seen that when  $x/y=1:0$ , all the diffraction peaks can be assigned to the orthorhombic LMP phase with  $\text{Pnmb}$  space group (JCPDS 74-0375). When  $x/y=0:1$ , the monoclinic LVP single-phase structure (space group  $\text{P2}_1/\text{n}$ , JCPDS 47-0107) can be observed. When  $x/y=8:1, 4:1, 2:1$  and  $1:1$ , the as-prepared composites are composed of orthorhombic LMP and monoclinic LVP phases without other impurities, and the relative diffraction peak intensity of  $\text{LMP} \cdot \text{LVP}$  decreases with the increase of LVP content. There is no evidence of diffraction peaks for crystalline carbon in all samples, indicating the state of carbon is amorphous. Fig. 11b shows the initial charge-discharge curves of the  $x\text{LMP} \cdot y\text{LVP/C}$  composites at 0.1 C in 2.4–4.8 V. Among all the  $x\text{LMP} \cdot y\text{LVP/C}$

## PERSPECTIVE

NJC

(x/y=8:1, 4:1, 2:1 and 1:1) composites, the LMP·LVP/C sample delivers the highest discharge capacity

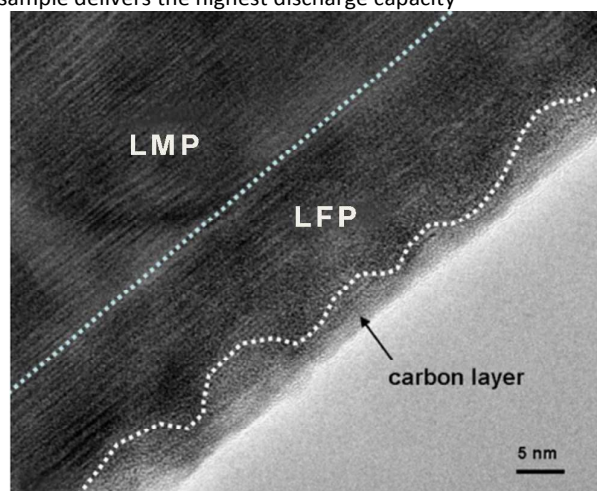


**Fig. 10** TEM image near the surface of a particle of the composite showing the different layers. Reproduced with permission from ref. 106. Copyright 2012 Elsevier.

of  $155 \text{ mAh g}^{-1}$ , about 48% higher than LMP/C ( $105 \text{ mAh g}^{-1}$ ). The enhanced performance is not only attributed to higher theoretical capacity of LVP (15.2% more), but also to higher utilization of LMP after compositing of highly conducting LVP nano-domains and V doping. The V doping into the host lattice of lithium transition-metal phosphates or forming composites may be an effective method to improve their electrochemical performances.<sup>108</sup> In order to improve the electrochemical performances of LMP cathode material, Qin et al.<sup>108</sup> prepared a series of  $(1-x)\text{LiMnPO}_4 \cdot x\text{Li}_3\text{V}_2(\text{PO}_4)_3/\text{C}$  [ $(1-x)\text{LMP} \cdot x\text{LVP}/\text{C}$ ] ( $x=0, 0.1, 0.2, 0.3, 0.4, 0.5$  and 1) composites through solid-state method using glucose as carbon source and reduction agent. For comparison, the  $(1-x)\text{LMP}+x\text{LVP}/\text{C}$  mixture with  $x=0.4$  was also prepared through mixing 60% LMP/C with 40% LVP/C. Fig. 12a shows the XRD patterns of the as-prepared  $(1-x)\text{LMP} \cdot x\text{LVP}/\text{C}$  samples and the  $(1-x)\text{LMP}+x\text{LVP}/\text{C}$  mixture with  $x=0.4$ . When  $x=0$ , all the diffraction peaks correspond well to the orthorhombic LMP phase with Pnmb space group (ICSD #25834). When  $x=0.1, 0.2, 0.3, 0.4$  and  $0.5$ , both the peaks of orthorhombic LMP and monoclinic LVP (space group  $\text{P}2_1/\text{n}$ , ICSD #96962) appear in the XRD patterns of the as-prepared materials. It can be seen that there is a noticeable difference in the characteristic peaks as the ratios of the two materials change. The diffraction peak intensity of LVP would gradually become stronger with increasing the content of LVP additives. However, for the samples with high LVP additives content ( $x=0.2, 0.3, 0.4, 0.5$  and 1), a few impurities are also observed, which could be indexed with a monoclinic  $\text{LiVP}_2\text{O}_7$  (LVP2) phase (ICSD #80551). Furthermore, it should be noted that the diffraction peaks of the  $0.6\text{LMP}+0.4\text{LVP}/\text{C}$  mixture in red line shifts (about  $0.13^\circ$ ) to the higher angle compared to that of the  $0.6\text{LMP} \cdot 0.4\text{LVP}/\text{C}$  composite. No obvious

diffraction peak of carbon is detected in all the samples, indicating the coated carbon is amorphous or the amount of carbon is too less to be measured. Fig. 12b shows the TEM images of

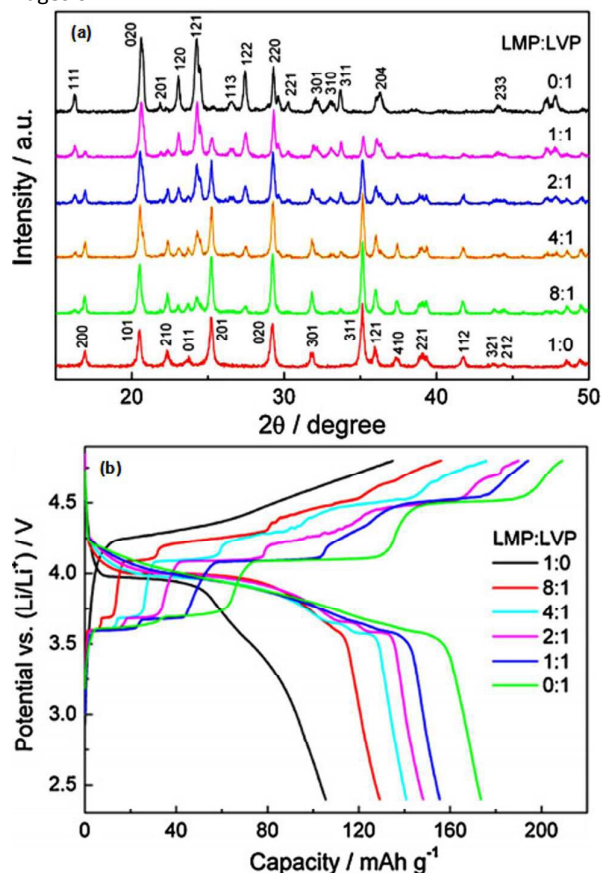


**Fig. 11** (a) XRD patterns of  $x\text{LMP} \cdot y\text{LVP}/\text{C}$  composites. (b) Initial charge-discharge curves of  $x\text{LMP} \cdot y\text{LVP}/\text{C}$  composites at 0.1 C in 2.4–4.8 V. Reproduced with permission from ref. 112. Copyright 2013 Elsevier.

$0.6\text{LMP} \cdot 0.4\text{LVP}/\text{C}$ . It can be seen that there are two kinds of lattice fringes in Fig. 12b, one is the lattice range of LMP (interplanar spacing 0.374 nm, lattice plane (101)), the other is the lattice fringe of LVP (interplanar spacing 0.365 nm, lattice plane (121), ICSD #96962). The lattice fringes become obscure on the particle boundaries between LMP and LVP, indicating the coexistence of both LMP and LVP phases. Fig. 12c shows the initial charge-discharge curves of  $(1-x)\text{LMP} \cdot x\text{LVP}/\text{C}$  ( $x=0, 0.1, 0.2, 0.3, 0.4, 0.5$  and 1) samples at 0.05 C rate in 2.0–4.5 V. It is obvious that with the amounts of LVP additives increase, the specific capacity of the composites increases. Among all the samples, the  $0.6\text{LMP} \cdot 0.4\text{LVP}/\text{C}$  composite shows the highest discharge capacity of  $154 \text{ mAh g}^{-1}$  at 0.05 C rate. The cycling performances of all the samples are shown in Fig. 12d and it was measured through charging at the rate of 0.2 and 0.5 C for discharging. The outstanding performances can be ascribed to the existence of the open

NJC

3D framework of the electronically conductive LVP phase and the doping V into the crystal structure of LMP.

More details about LVP-LMP hybrid cathode materials for LIBs are summarized in Table 2.

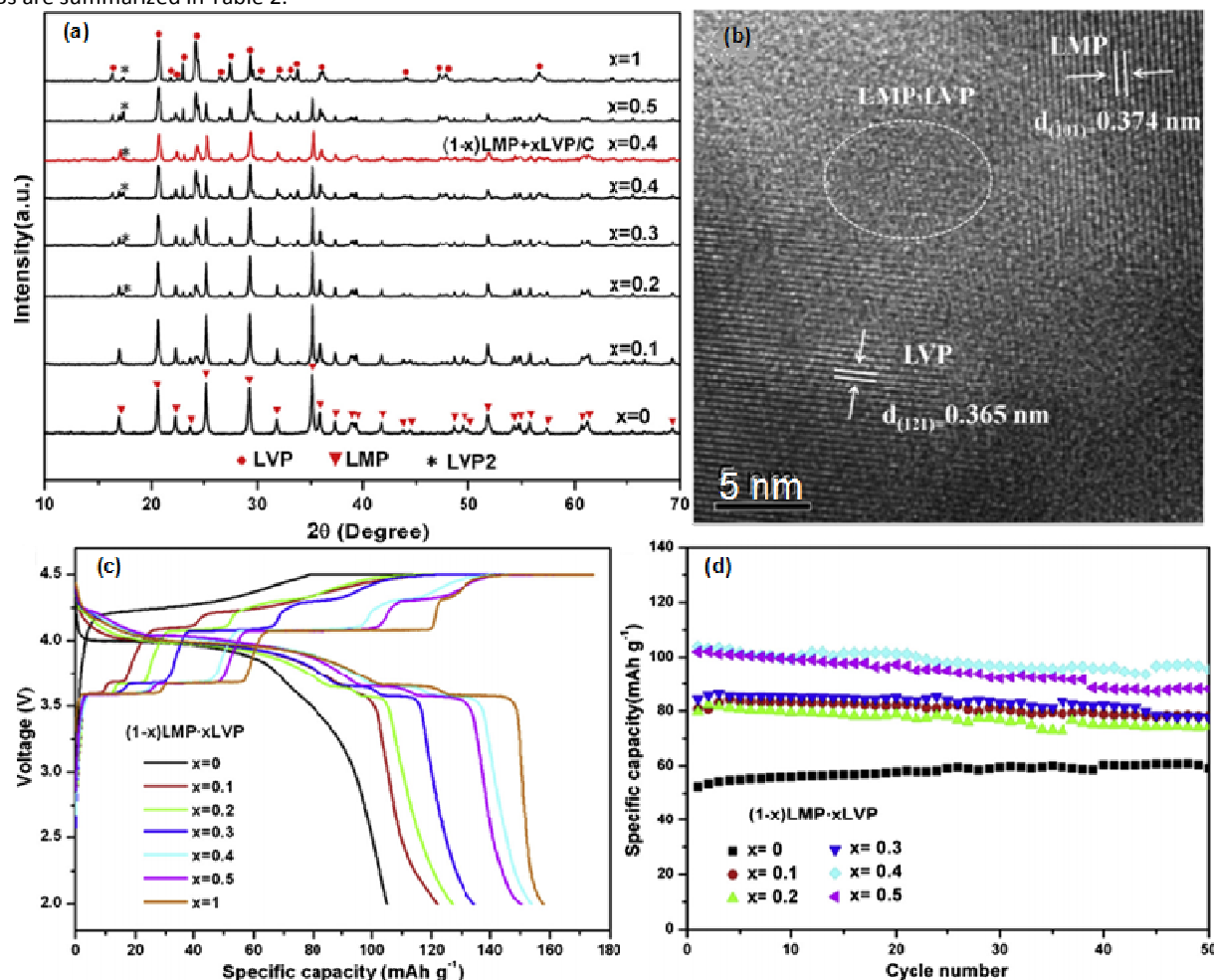


**Fig. 12** (a) XRD patterns of the as-prepared  $(1-x)\text{LMP} \cdot x\text{LVP}/\text{C}$  samples and the  $(1-x)\text{LMP}+x\text{LVP}/\text{C}$  mixture with  $x=0.4$ . (b) TEM image of  $0.6\text{LMP} \cdot 0.4\text{LVP}/\text{C}$ . (c) Initial charge-discharge curves of  $(1-x)\text{LMP} \cdot x\text{LVP}/\text{C}$  ( $x=0, 0.1, 0.2, 0.3, 0.4, 0.5$  and  $1$ ) samples at  $0.05\text{ C}$  rate from  $2.0$  to  $4.5\text{ V}$ . (d) Cycling performances of all the samples charging at the rate of  $0.2$  and  $0.5\text{ C}$  for discharging in  $2.0 - 4.5\text{ V}$ . Reproduced with permission from ref. 108. Copyright 2013 Elsevier.

**Table 2** LVP-LMP hybrid cathode materials for LIBs.

Molar ratio	Preparation method	Electrochemical performances	References
LMP:LVP=1:2	Mechanochemical process	Initial discharge capacity of $154.0\text{ mAh g}^{-1}$ at $C/50$ in $2.5-4.8\text{ V}$ at $55^\circ\text{ C}$ .	113
LMP:LVP=4:1	High temperature solid-state reaction	Initial discharge capacity of $121.5\text{ mAh g}^{-1}$ at $0.05\text{ C}$ in $2.5-4.4\text{ V}$ .	114
LMP:LVP=4:1-1:1	High temperature solid-state reaction	Capacity of $\sim 125\text{ mAh g}^{-1}$ at $0.05\text{ C}$ in $2.5-4.4\text{ V}$ .	115
LMP:LVP=1:1	Aqueous precipitation for the first time, followed by chemical reduction and lithiation	Initial discharge capacities of $110, 104.4, 100.6$ and $80.4\text{ mAh g}^{-1}$ at $0.1, 1, 3$ and $10\text{ C}$ , respectively.	116

LMP has similar structure and theoretical capacity with LFP, but can provide higher working potential and energy density

than LFP. However, LFP has achieved industrialization and LMP still remains in the phase of theoretical research. Much

more work still need to be done for cathode materials contain Mn due to their intrinsic defects. It is necessary to noted that LVP and LMP both have a voltage platform at 4.1 V, so the charge-discharge curves may overlap at this voltage.

LMP seems to have brighter future than LFP, the future work should focus on the modification.

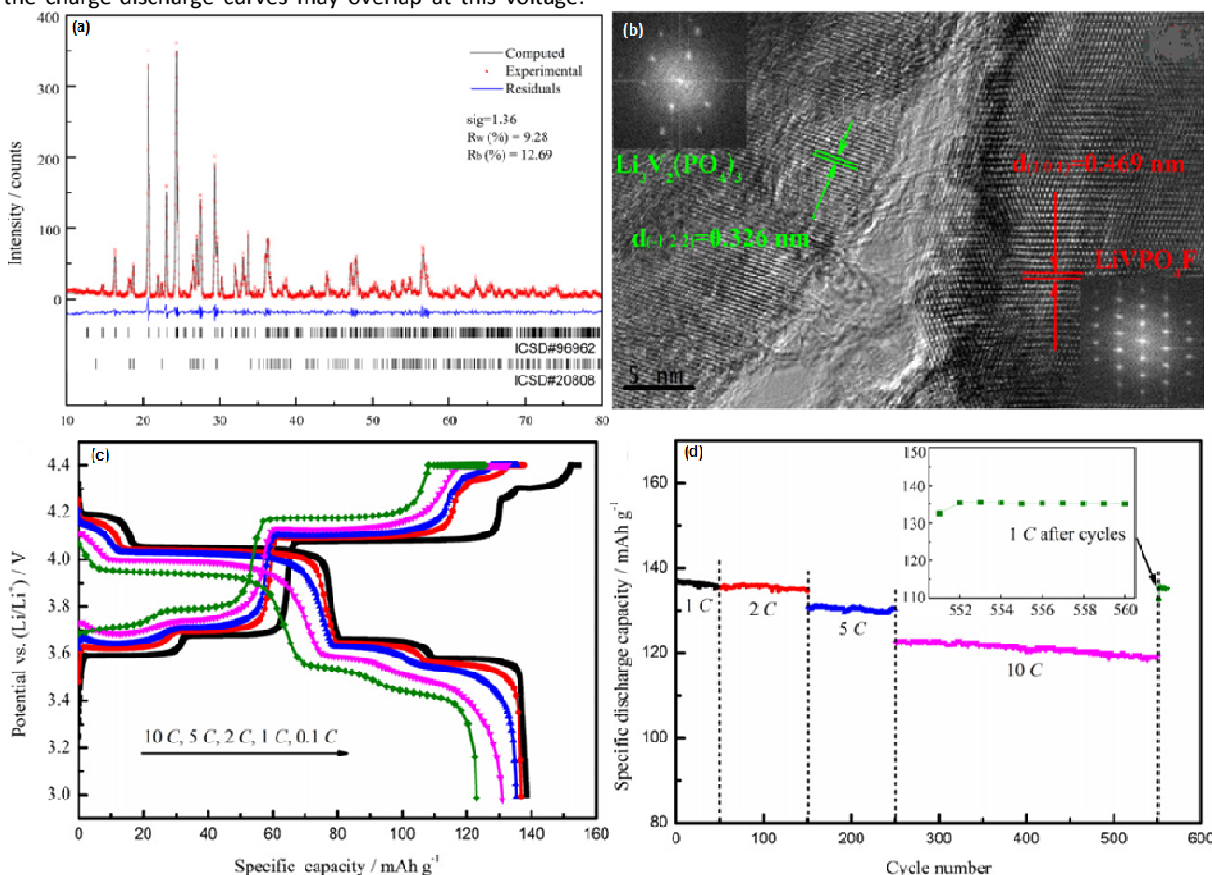


**Fig. 13** (a) Multiphase refinement for powder XRD patterns of the prepared composite. (b) HRTEM image together with the inset FFT of the prepared composite. (c) The initial charge-discharge curves of Li/xLVP-LVPF half cell at various rates in 3.0 – 4.4 V. (d) Cycling performances of Li/xLVP-LVPF half cell at various rates. Reproduced with permission from ref. 119. Copyright 2013 Elsevier.

### $\text{Li}_3\text{V}_2(\text{PO}_4)_3\text{-LiVPO}_4\text{F}$

In recent years, framework-structured Li-containing fluorophosphates of d-metals such as  $\text{LiVPO}_4\text{F/C}$  (LVPF/C) have been explored as perspective high-voltage cathode materials for rechargeable LIBs.<sup>117</sup> Triclinic structure lithium vanadium fluorophosphate with chemical formula of  $\text{LiVPO}_4\text{F}$  was first reported by Barker et al.<sup>118</sup> Because of the impact of structural fluorine on the inductive effect of the  $\text{PO}_4^{3-}$  polyanion,  $\text{V}^{3+}/\text{V}^{4+}$  redox couple in LVPF is located at a high potential of about 4.2 V, which is about 0.3 V higher than the average potential for the same transition ( $\text{V}^{3+}/\text{V}^{4+}$ ) in the lithium vanadium phosphate, LVP.<sup>118</sup> Furthermore, LVPF exhibits higher electronic conductivity than traditional phosphates such as LFP, LMP and  $\text{LiVOPO}_4$ .<sup>100</sup> Considering the advantages of LVP and LVPF, Wang et al.<sup>119</sup> synthesized xLVP-LVPF/C composite coated with carbon via mechanically activated chemical reduction followed by annealing. The

value of x is designed to be 2.0 but in fact is 2.7 in the prepared sample because of volatilization of HF or  $\text{VF}_3$ . Fig. 13a shows the structure characterization of the prepared material, which was carried out with powder X-ray diffraction. It can be seen that two phases of LVP and LVPF are detected, and without other undesired phases such as LiF or  $\text{V}_2\text{O}_3$ . Fig. 13b shows the morphology of the prepared sample. Grain boundary of crystalline LVP and LVPF can be seen clearly in Fig. 13b, indicating that the LVP and LVPF crystals inset into each other well in the prepared composite. Fig. 13c shows the initial charge-discharge curves of Li/xLVP-LVPF half cell at various rates in 3.0–4.4 V. The initial discharge capacities are 139, 137, 135, 131 and 123  $\text{mAh g}^{-1}$  at 0.1, 1, 2, 5 and 10 C, respectively. Fig. 13d shows the cycling performances of Li/xLVP-LVPF half cell at various rates. It can be seen that the cell retains 98.9%, 99.5%, 99.5% and 97.3% of its initial discharge capacity after 50, 100, 100 and 300 cycles at 1, 2, 5 and 10 C, respectively. Furthermore, after 300 cycles at 10 C, only a slight capacity fading at 1 C is

NJC

obtained. The good electrochemical performance of the synthesized sample is attributed to synergistic effect of LVP-LVOP composite, as well as carbon coating.

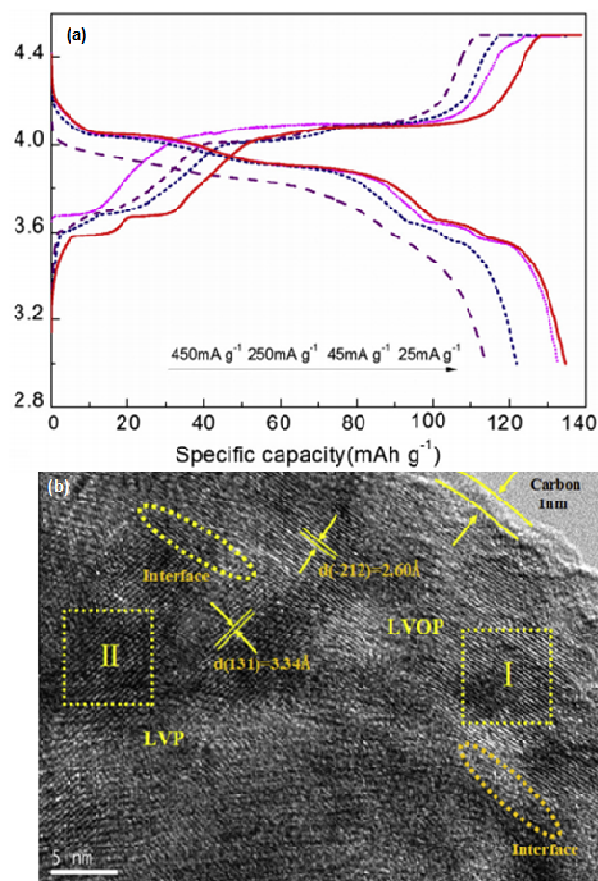


**Fig. 14** (a) The charge-discharge profiles of LVOP-LVP sample synthesized for 2 h at different current density in 3.0 – 4.5 V. (b) TEM image of LVOP-LVP (2 h) sample. Reproduced with permission from ref. 120. Copyright 2015 Elsevier.

As mentioned before, the synthetic condition of LVOP is strict. Furthermore, it is hard to get desired proportion (LVP and LVOP), because the content of F is easy to decrease in the synthesis process of LVOP. How to control the loss of F may be the first step. Future workers should also pay attention to the safety problem caused by V or F, especially for the body.

#### $\text{Li}_3\text{V}_2(\text{PO}_4)_3\text{-LiVOPO}_4$

$\text{LiVOPO}_4$  (LVOP) is a potential contender for high voltage cathode material due to high theoretical capacity of  $166 \text{ mAh g}^{-1}$ , higher lithium intercalation potential of nearly 4 V and high theoretical energy density.<sup>120</sup> However, only part of the capacity could be obtained for LVOP, and its capacity decreases considerably for the low electrical conductivity and Li ion diffusion.<sup>121</sup> LVP is often used as an additive to enhance the conductivity of cathode materials which have low conductivity due to its fast ionic conduction in the bulk

materials.<sup>59,68,122-124</sup> Recently, Shen et al.<sup>120</sup> synthesized a series of multi-layered core-shell LVOP-LVP composites through a two-stage sintering method. The precursor was firstly sintered at  $700^\circ \text{C}$  for 10 h under an inert atmosphere to form LVP. Then, the inert atmosphere was removed until the temperature dropped to  $350^\circ \text{C}$ . Finally, the as-prepared LVP was sintered at  $350^\circ \text{C}$  for different time in the air atmosphere. The formation of LVOP-LVP was by partly transformation of LVP to LVOP from the surface to the internal of the particles, and the valence state of the V element was changed from +4 to +3 along the direction from outside to inside of the particles. The LVOP-LVP composite synthesized for 2 h in air shows the best electrochemical performance with a discharge capacity of  $132.8 \text{ mAh g}^{-1}$  at  $45 \text{ mA g}^{-1}$  in 3.0–4.5 V, and the capacity was  $126.8 \text{ mAh g}^{-1}$  after 100 cycles. The charge-discharge profiles of LVOP-LVP sample synthesized for 2 h at different current density in 3.0–4.5 V are shown in Fig. 14a. It can be seen that the cells of LVOP-LVP exhibit four plateaus, with three plateaus for LVP and the other one for LVOP. Fig. 14b shows the TEM image of LVOP-LVP (2 h) composite. Two kinds of lattice fringes corresponding to LVOP(I) and LVP(II) co-existed in the composites. The lattice fringe of LVOP with an interplanar spacing of  $2.60 \text{ \AA}$  is in accordance with the (-212) lattice planes, and the other  $2.60 \text{ \AA}$  one is corresponding to the (131) lattice planes of LVP. The HRTEM images provide a clearly scene of the coexistence of the three phases: LVOP, LVP and amorphous carbon, forming a multi-layered core-shell structure, while the core is LVP, the external shell is the 1 nm-sized amorphous carbon, and the internal shell is LVOP.

Just like LFP-LMO hybrid cathode materials, two atmospheres (air and inert) are required to get LVOP-LVP composite. Two atmospheres usually increase the complexity of the experiment and may be hard to control.

#### $\text{LiCoO}_2\text{-LiMn}_2\text{O}_4$

As LCO has a higher electric conductivity than LMO, so it is possible to improve the rate capability of LMO. In order to enhance the rate capability of LMO, Park et al.<sup>125</sup> prepared LCO-LMO composite. The surface of LMO particle was coated with LCO by a sol-gel method. After the surface coating, LCO-coated LMO showed a higher discharge capacity of  $120 \text{ mAh g}^{-1}$  than as-received LMO ( $115 \text{ mAh g}^{-1}$ ), because LCO has a higher capacity than LMO. Besides, a series of LCO-LMO composites have been successfully synthesized in recent years, and they show excellent performance in some respects.<sup>126-129</sup>

### Conclusions and prospectives

Hybrid cathode materials are a composite consisting of two or more cathode materials and have been reported a lot in recent years. The current research focuses mainly on the LFP-LVP hybrid cathode materials, since the advantages of LFP or LVP are really attractive. However, compared to single

cathode material, there is less systematic research on the technological innovation of hybrid cathode materials in the present. In particular, the development of its theoretical study is slower because the synthesis of hybrid cathode materials have many inner and external influence factors.

Further more work still need to be done to achieve the commercialization of hybrid cathode materials. Challenges and problems still exist in the research, such as the mechanism of mixing doping, the best mixing methods, how to get the optimal proportion, how to calculate the current density in the charge-discharge process, how to ensure the uniformity, and so on. Further work should pay more attention to synthesis mechanism and the mixing process, because in which step to mix has great effects on the electrochemical performances. The future workers should also study carefully of each cathode and consider the possibility before synthesizing hybrid cathode materials. Besides, the mixing of three or more cathode materials still need to be studied. With the deepening of the research, we believe all the problems will be resolved.

### Acknowledgements

The authors thank the Natural Science Foundation of China (Grant no. 51272144, 51472127 and 51172132) for financial support. They also thank Shandong Provincial Key Laboratory of Processing and Testing Technology of Glass and Functional Ceramics for technological support.

### Notes and references

- 1 C. Wei, W. He, X. Zhang, S. Liu, C. Jin, S. Liu, Z. Huang, *RSC Adv.*, 2015, 5, 28662-28669.
- 2 M. S. Whittingham, *Chem. Rev.*, 2004, 104, 4271-4302.
- 3 L. Su, Y. Jing, Z. Zhou, *Nanoscale*, 2011, 3, 3967-3983.
- 4 X. Rui, Q. Yan, M. Skyllas-Kazacos, T. M. Lim, *J. Power Sources*, 2014, 258, 19-38.
- 5 S. Wang, Z. Zhang, A. Deb, L. Yang, S. i. Hirano, *Ind. Eng. Chem. Res.*, 2014, 53, 19525-19532.
- 6 T. Wei, R. Zeng, Y. Sun, Y. Huang, K. Huang, *Chem. Commun.*, 2014, 50, 1962-1964.
- 7 Y. Bai, K. Jiang, S. Sun, Q. Wu, X. Lu, N. Wan, *Electrochim. Acta*, 2014, 134, 347-354.
- 8 J. Yu, Z. Han, X. Hu, H. Zhan, Y. Zhou, X. Liu, *J. Power Sources*, 2014, 262, 136-139.
- 9 T. Azib, F. Le Cras, H. Porthault, *Electrochim. Acta*, 2015, 160, 145-151.
- 10 W. Sun, M. Xie, X. Shi, L. Zhang, *Mater. Res. Bull.*, 2015, 61, 287-291.
- 11 Z. Wang, Z. Wang, H. Guo, W. Peng, X. Li, *J. Alloy. Compd.*, 2015, 626, 228-233.
- 12 L. Xia, Y. Xia, Z. Liu, *Electrochim. Acta*, 2015, 151, 429-436.
- 13 X. Gao, Y. Sha, Q. Lin, R. Cai, M. O. Tade, Z. Shao, *J. Power Sources*, 2015, 275, 38-44.
- 14 Y. Shang, X. Lin, X. Lu, T. Huang, A. Yu, *Electrochim. Acta*, 2015, 156, 121-126.
- 15 H. Zhang, Y. Xu, D. Liu, *RSC Adv.*, 2015, 5, 11091-11095.
- 16 F. Zhou, P. Zhu, X. Fu, R. Chen, R. Sun, C. Wong, *CrystEngComm*, 2014, 16, 766-774.
- 17 H. Guo, C. Wu, J. Xie, S. Zhang, G. Cao, X. Zhao, *J. Mater. Chem. A*, 2014, 2, 10581-10588.
- 18 Q. Xia, T. Liu, J. Xu, X. Cheng, W. Lu, X. Wu, *J. Mater. Chem. A*, 2015, 3, 6301-6305.
- 19 D. G. Kellerman, Yu. G. Chukalkin, N. I. Medvedeva, M. V. Kuznetsov, N. A. Mukhina, A. S. Semenova, V. S. Gorshkov, *Mater. Chem. Phys.*, 2015, 149-150, 209-215.
- 20 Y. Gu, H. Wang, Y. Zhu, L. Wang, Y. Qian, Y. Chu, *Solid State Ionics*, 2015, 274, 106-110.
- 21 P. Zhang, H. Wang, Q. Si, M. Matsui, Y. Takeda, O. Yamamoto, N. Imanishi, *Solid State Ionics*, 2015, 272, 101-106.
- 22 A. Svitan'ko, V. Scopets, S. Novikova, A. Yaroslavtsev, *Solid State Ionics*, 2015, 271, 42-47.
- 23 P. Zhang, M. Matsui, Y. Takeda, O. Yamamoto, N. Imanishi, *Solid State Ionics*, 2014, 263, 27-32.
- 24 C. Fan, C. Lin, S. Han, J. Chen, L. Li, Y. Bai, K. Zhang, X. Zhang, *New J. Chem.*, 2014, 38, 795-801.
- 25 X. Li, H. Jin, S. Liu, S. Xin, Y. Meng, J. Chen, *J. Mater. Chem. A*, 2015, 3, 116-120.
- 26 N. Delaporte, A. Perea, R. Amin, K. Zaghbi, D. Bélanger, *J. Power Sources*, 2015, 280, 246-255.
- 27 Z. Zhang, Z. Zhang, W. Chen, G. Wang, J. Li, Y. Lai, *New J. Chem.*, 2015, 39, 3765-3769.
- 28 F. Yu, L. Zhang, L. Lai, M. Zhu, Y. Guo, L. Xia, P. Qi, G. Wang, B. Dai, *Electrochim. Acta*, 2015, 151, 240-248.
- 29 J. Zhang, J. Wang, Y. Liu, N. Nie, J. Gu, F. Yu, W. Li, *J. Mater. Chem. A*, 2015, 3, 2043-2049.
- 30 M. Liu, Y. Zhao, S. Gao, Y. Wang, Y. Duan, X. Han, Q. Dong, *New J. Chem.*, 2015, 39, 1094-1100.
- 31 Y. Xie, F. Song, C. Xia, H. Du, *New J. Chem.*, 2015, 39, 604-613.
- 32 B. Wang, A. Liu, W. A. Abdulla, D. Wang, X. S. Zhao, *Nanoscale*, 2015, 7, 8819-8828.
- 33 M. M. Majdabadi, S. Farhad, M. Farkhondeh, R. A. Fraser, M. Fowler, *J. Power Sources*, 2015, 275, 633-643.
- 34 C. Fan, S. Han, K. Zhang, L. Li, X. Zhang, *New J. Chem.*, 2014, 38, 4336-4343.
- 35 C. Wang, W. Shen, H. Liu, *New J. Chem.*, 2014, 38, 430-436.
- 36 M. S. Choi, H. S. Kim, Y. M. Lee, B. S. Jin, *J. Mater. Chem. A*, 2014, 2, 7873-7879.
- 37 X. Zhang, R. S. Kühnel, H. Hu, D. Eder, A. Balducci, *Nano Energy*, 2015, 12, 207-214.
- 38 C. Lai, J. Wei, Z. Wang, Q. Xu, Y. Lu, H. Li, *Solid State Ionics*, 2015, 272, 121-126.
- 39 C. Lai, Z. Chen, H. Zhou, Y. Lu, H. Li, *J. Mater. Sci.*, 2015, 50, 3075-3082.
- 40 M. Choi, H. S. Kim, Y. M. Lee, B. S. Jin, *Mater. Lett.*, 2015, 145, 83-86.
- 41 M. M. Ren, Z. Zhou, X. P. Gao, W. X. Peng, J. P. Wei, *J. Phys. Chem. C*, 2008, 112, 5689-5693.
- 42 Y. Piao, Y. Qin, Y. Ren, S. M. Heald, C. Sun, D. Zhou, B. J. Polzin, S. E. Trask, K. Amine, Y. Wei, G. Chen, I. Bloom, Z. Chen, *Phys. Chem. Chem. Phys.*, 2014, 16, 3254-3260.
- 43 X. Sun, Y. Xu, M. Jia, P. Ding, Y. Liu, K. Chen, *J. Mater. Chem. A*, 2013, 1, 2501-2507.
- 44 C. Ling, R. Zhang, F. Mizuno, *J. Mater. Chem. A*, 2014, 2, 12330-12339.
- 45 C. Shen, B. Zhang, J. F. Zhang, J. C. Zheng, Y. D. Han, H. Li, *RSC Adv.*, 2015, 5, 7208-7214.
- 46 M. M. Ren, Z. Zhou, X. P. Gao, L. Liu, W. X. Peng, *J. Phys. Chem. C*, 2008, 112, 13043-13046.
- 47 A. K. Padhi, K. S. Nanjundaswamy, J. B. Goodenough, *J. Electrochem. Soc.*, 1997, 144, 1188-1194.
- 48 Y. Guo, Y. Huang, D. Jia, X. Wang, N. Sharma, Z. Guo, X. Tang, *J. Power Sources*, 2014, 246, 912-917.
- 49 D. Morgan, A. Van der Ven, G. Ceder, *Electrochem. Solid-State Lett.*, 2004, 7, A30-A32.

NJC

- 50 X. Wang, Y. Huang, D. Jia, Z. Guo, D. Ni, M. Miao, J. Solid State Electrochem., 2012, 16, 17-24.
- 51 Y. H. Huang, J. B. Goodenough, Chem. Mater., 2008, 20, 7237-7241.
- 52 B. L. Ellis, K. T. Lee, L. F. Nazar, Chem. Mater., 2010, 22, 691-714.
- 53 S. Ferrari, R. L. Lavall, D. Capsoni, E. Quartarone, A. Magistris, P. Mustarelli, P. Canton, J. Phys. Chem. C, 2010, 114, 12598-12603.
- 54 Y. Qiao, L. Pan, L. He, L. Dumée, L. Kong, M. Zhao, L. Wang, W. Gao, Ionics, 2015, 21, 295-299.
- 55 Y. Liu, J. Gu, J. Zhang, F. Yu, J. Wang, N. Nie, W. Li, RSC Adv., 2015, 5, 9745-9751.
- 56 R. Tian, G. Liu, H. Liu, L. Zhang, X. Gu, Y. Guo, H. Wang, L. Sun, W. Chu, RSC Adv., 2015, 5, 1859-1866.
- 57 W. F. Howard, R. M. Spotnitz, J. Power Sources, 2007, 165, 887-891.
- 58 M. Y. Saïdi, J. Barker, H. Huang, J. L. Swoyer, G. Adamson, J. Power Sources, 2003, 119-121, 266-272.
- 59 S. C. Yin, H. Grondey, P. Strobel, M. Anne, L. F. Nazar, J. Am. Chem. Soc., 2003, 125, 10402-10411.
- 60 S. Patoux, C. Wurm, M. Morcrette, G. Rousse, C. Masquelier, J. Power Sources, 2003, 119-121, 278-284.
- 61 J. Barker, R. K. B. Gover, P. Burns and A. Bryan, J. Electrochem. Soc., 2007, 154, A307-A313.
- 62 H. Huang, S. C. Yin, T. Kerr, N. Taylor, L. F. Nazar, Adv. Mater., 2002, 14, 1525-1528.
- 63 S. C. Yin, H. Grondey, P. Strobel, M. Anne, L. F. Nazar, J. Am. Chem. Soc., 2003, 125, 10402-10411.
- 64 G. Yang, H. Liu, H. Ji, Z. Chen, X. Jiang, Electrochim. Acta, 2010, 55, 2951-2957.
- 65 M. Manickam, M. Takata, Electrochim. Acta, 2003, 48, 957-963.
- 66 H. Huang, T. Faulkner, J. Barker, M. Y. Saidi, J. Power Sources, 2009, 189, 748-751.
- 67 M. E. Zhong, Z. H. Zhou, Z. T. Zhou, The Chinese Journal of Nonferrous Metals, 2009, 19, 1462-1467.
- 68 J. C. Zheng, X. H. Li, Z. X. Wang, J. H. Li, L. J. Li, H. J. Guo, Ionics, 2009, 15, 753-759.
- 69 C. Gao, H. Liu, G. Liu, J. Zhang, W. Wang, Mat. Sci. Eng. B, 2013, 178, 272-276.
- 70 J. Y. Xiang, J. P. Tu, L. Zhang, X. L. Wang, Y. Zhou, Y. Q. Qiao, Y. Lu, J. Power Sources, 2010, 195, 8331-8335.
- 71 J. C. Zheng, X. H. Li, Z. X. Wang, S. S. Niu, D. R. Liu, L. Wu, L. J. Li, J. H. Li, H. J. Guo, J. Power Sources, 2010, 195, 2935-2938.
- 72 D. H. Kim, J. Kim, Electrochem. Solid-State Lett., 2006, 9, A439-A442.
- 73 M. R. Yang, W. h. Ke, S. h. Wu, J. Power Sources, 2007, 165, 646-650.
- 74 L. Wang, Z. Li, H. Xu, K. Zhang, J. Phys. Chem. C, 2008, 112, 308-312.
- 75 S. Zhong, W. Chen, L. Wu, J. Liu, Ionics, 2012, 18, 523-527.
- 76 H. Tang, X. D. Guo, B. H. Zhong, H. Liu, Y. Tang, R. Xu, L. Y. Li, J. Solid State Electr., 2012, 16, 1537-1543.
- 77 S. Zhong, L. Wu, J. Zheng, J. Liu, Powder Technol., 2012, 219, 45-48.
- 78 S. Zhong, L. Wu, J. Liu, Electrochim. Acta, 2012, 74, 8-15.
- 79 X. Zhang, H. Guo, X. Li, Z. Wang, L. Wu, Solid State Ionics, 2012, 212, 106-111.
- 80 Z. Ma, G. Shao, X. Wang, J. Song, G. Wang, Ionics, 2013, 19, 1861-1866.
- 81 L. Wu, J. Lu, S. Zhong, J. Solid State Electr., 2013, 17, 2235-2241.
- 82 J. F. Zhang, C. Shen, B. Zhang, J. C. Zheng, C. L. Peng, X. W. Wang, X. B. Yuan, H. Li, G. M. Chen, J. Power Sources, 2014, 267, 227-234.
- 83 H. Wang, W. D. Zhang, L. Y. Zhu, M. C. Chen, Solid State Ionics, 2007, 178, 131-136.
- 84 H. S. Kim, M. Kong, K. Kim, I. J. Kim, H. B. Gu, J. Electroceram., 2009, 23, 219-224.
- 85 J. M. Tarascon, M. Armand, Nature, 2001, 414, 359-367.
- 86 K. Xu, Chem. Rev., 2004, 104, 4303-4418.
- 87 F. Zhou, X. M. Zhao, A. V. Bommel, X. Xia, J. R. Dahn, J. Electrochem. Soc., 2011, 158, 81-87.
- 88 Y. Kim, G. M. Veith, J. Nanda, R. R. Unocic, M. Chi, N. J. Dudney, Electrochim. Acta, 2011, 56, 6573-6580.
- 89 T. Yang, N. Zhang, Y. Lang, K. Sun, Electrochim. Acta, 2011, 56, 4058-4064.
- 90 J. H. Kim, C. W. Park, Y. K. Sun, Solid State Ionics, 2003, 164, 43-49.
- 91 B. Sadeghi, R. Sarraf-Mamoory, H. R. Shahverdi, J. Nanomater., 2012, 2012, 743236, 7 pages.
- 92 X. Li, Y. Xu, J. Solid State Electr., 2008, 12, 851-855.
- 93 Y. Xia, N. Kumada, M. Yoshio, J. Power Sources, 2000, 90, 135-138.
- 94 G. R. Hu, X. R. Deng, Z. D. Peng, K. Du, Electrochim. Acta, 2008, 53, 2567-2573.
- 95 C. Qiu, L. Liu, F. Du, X. Yang, C. Wang, G. Chen, Y. Wei, Chem. Res. Chin. Univ., 2015, 31, 270-275.
- 96 P. Li, R. Ma, X. Lin, L. Shao, K. Wu, M. Shui, N. Long, J. Shu, J. Alloy. Compd., 2015, 637, 20-29.
- 97 J. C. Zheng, Y. D. Han, B. Zhang, C. Shen, L. Ming, J. F. Zhang, ACS Appl. Mater. Interfaces, 2014, 6, 13520-13526.
- 98 X. Sun, Y. Xu, G. Chen, P. Ding, X. Zheng, Solid State Ionics, 2014, 268, 236-241.
- 99 J. M. Ateba Mba, L. Croguennec, N. I. Basir, J. Barker, C. Masquelier, J. Electrochem. Soc., 2012, 159, A1171-A1175.
- 100 J. Barker, R. K. B. Gover, P. Burns, A. Bryan, M. Y. Saidi, J. L. Swoyer, J. Power Sources, 2005, 146, 516-520.
- 101 Y. C. Lin, G. T. Kuo Fey, P. J. Wu, J. K. Chang, H. M. Kao, J. Power Sources, 2013, 244, 63-71.
- 102 F. Zhou, X. Zhao, J. R. Dahn, Electrochem. Commun., 2009, 11, 589-591.
- 103 Y. Liu, Y. Xu, X. Sun, Funct. Mater. Lett., 2013, 6, 1350053, 4 pages.
- 104 R. Ma, L. Shao, K. Wu, M. Shui, D. Wang, N. Long, Y. Ren, J. Shu, J. Power Sources, 2014, 248, 874-885.
- 105 S. Hamelet, P. Gibot, M. Casas-Cabanas, D. Bonnin, C. P. Grey, J. Cabana, J. B. Leriche, J. Rodriguez-Carvajal, M. Courty, S. Levasseur, P. Carlach, M. V. Thournout, J. M. Tarascon, C. Masquelier, J. Mater. Chem., 2009, 19, 3979-3991.
- 106 K. Zaghbi, M. Trudeau, A. Guerfi, J. Trottier, A. Mauger, R. Veillette, C. M. Julien, J. Power Sources, 2012, 204, 177-181.
- 107 J. Bai, J. Hong, H. Chen, J. Graetz, F. Wang, J. Phys. Chem. C, 2015, 119, 2266-2276.
- 108 L. Qin, Y. Xia, B. Qiu, H. Cao, Y. Liu, Z. Liu, J. Power Sources, 2013, 239, 144-150.
- 109 C. Delacourt, L. Laffont, R. Bouchet, C. Wurm, J.B. Leriche, M. Morcrette, J.M. Tarascon, C. Masquelier, J. Electrochem. Soc., 2005, 152, A913-A921.
- 110 A. Yamada, Y. Kudo, K.Y. Liu, J. Electrochem. Soc., 2001, 148, A1153-A1158.
- 111 N. Meethong, H.Y.S. Huang, S.A. Speakman, W.C. Carter, Y.M. Chiang, Adv. Funct. Mater., 2007, 17, 1115-1123.
- 112 F. Wang, J. Yang, Y. NuLi, J. Wang, Electrochim. Acta, 2013, 103, 96-102.
- 113 J. S. Yun, S. Kim, B. W. Cho, K. Y. Lee, K. Y. Chung, W. Chang, Bull. Korean Chem. Soc., 2013, 34, 433-436.
- 114 Y. Bi, W. Yang, B. Yang, C. Wang, D. Wang, S. Shi, Ceram. Int., 2014, 40, 7637-7641.

## PERSPECTIVE

NJC

- 115 C. Wang, Y. Bi, Y. Liu, Y. Qin, Y. Fang, D. Wang, *J. Power Sources*, 2014, 263, 332-337.
- 116 B. Zhang, X. W. Wang, J. F. Zhang, *RSC Adv.*, 2014, 4, 49123-49127.
- 117 N. V. Kosova, E. T. Devyatkina, A. B. Slobodyuk, A. K. Gutakovskii, *J. Solid State Electr.*, 2014, 18, 1389-1399.
- 118 J. Barker, M. Y. Saidi, J. L. Swoyer, *J. Electrochem. Soc.*, 2003, 150, A1394-A1398.
- 119 J. Wang, Z. Wang, X. Li, H. Guo, X. Wu, X. Zhang, W. Xiao, *Electrochim. Acta*, 2013, 87, 224-229.
- 120 C. Shen, B. Zhang, J. C. Zheng, Y. D. Han, J. F. Zhang, *J. Alloy. Comp.*, 2015, 622, 771-776.
- 121 M. M. Ren, Z. Zhou, L.W. Su, X. P. Gao, *J. Power Sources*, 2009, 189, 786-789.
- 122 D. Morgan, G. Ceder, M. Y. Saidi, J. Swoyer, H. Huang, G. Adamson, *Chem. Mater.*, 2002, 14, 4684-4693.
- 123 J. Gaubicher, C. Wurm, G. Goward, C. Masquelier, L. Nazar, *Chem. Mater.*, 2000, 12, 3240-3242.
- 124 M. Sato, H. Ohkawa, K. Yoshida, M. Saito, K. Uematsu, K. Toda, *Solid State Ionics*, 2000, 135, 137-142.
- 125 S. C. Park, Y. M. Kim, Y. M. Kang, K. T. Kim, P. S. Lee, J. Y. Lee, *J. Power Sources*, 2001, 103, 86-92.
- 126 Z. Liu, H. Wang, L. Fang, J. Y. Lee, L. M. Gan, *J. Power Sources*, 2002, 104, 101-107.
- 127 N. V. Kosova, E. T. Devyatkina, V. V. Kaichev, *Russ. J. Electrochem.*, 2009, 45, 277-285.
- 128 E. V. Makhonina, Y. V. Shatilo, V. S. Dubasova, A. F. Nikolenko, T. A. Ponomareva, E. V. Kisterev, V. S. Pervov, *Inorg. Mater.*, 2009, 45, 935-941.
- 129 H. E. Wang, D. Qian, Z. G. Lu, Y. K. Li, *J. Alloy. Comp.*, 2012, 517, 186-191.

**TABLE OF CONTENT (TOC).** Various binary composite cathode materials for lithium ion batteries are summarized and discussed.

